Measurements of the frequency dependence of normal modes

C. T. Tindle, K. M. Guthrie,[a] G. E. J. Bold, M. D. Johns, D. Jones, K. O. Dixon,[a] and T. G. Birdsall[b]

Physics Department, University of Auckland, Auckland, New Zealand

(Received 25 October 1977; revised 17 April 1978)

An experiment using a vertical array to detect acoustic normal modes in shallow water is described. A high signal-to-noise ratio was achieved by the use of pseudorandom pulse sequences to modulate the projector. Wide bandwidth signals and a tunable acoustic source enabled the frequency dependence of normal modes to be measured and results are in good agreement with the theory. An improved method of extracting the signal present in a single mode is described and used to examine pulse shapes and frequency spectra of individual modes.

PACS numbers: 43.30.Sf, 43.30.Jx

INTRODUCTION

The analysis of underwater acoustic signals in terms of normal modes began with the work of Pekeris in 1948.[1] Since then, the theory of acoustic normal modes has been successfully used to interpret a wide variety of experimental results.

The direct observation of the depth-dependence characteristics of normal modes was reported recently in the work of Ferris[2] and Ingenito.[3] The essential feature of their experiment was the use of a vertical string of hydrophones spaced evenly throughout the water depth. Sampling of the acoustic field in this way allows the observation of the phase and amplitude variation with depth, and Ferris and Ingenito were able to identify two normal modes and to measure their attenuation.

The fundamental property of propagation of an acoustic signal carried by normal modes is that the vertical distribution of energy in a given normal mode takes up a standing wave pattern. For a range-independent environment this standing wave pattern remains unchanged as the signal propagates horizontally away from the source. The signal present in a given mode starts off as a replica of the source signal but because pulses in different modes travel at different speeds a received signal usually shows several arrivals. These arrivals may overlap in which case the signal is difficult to interpret.

It is of obvious interest to be able to extract the signal present in a single normal mode since, if the effects of dispersion are not too great, a replica of the source signal can be obtained from a complicated multiple-arrival record. The basic experimental arrangement of Ferris and Ingenito allows the possibility of extracting mode signals and has been used for the present work.

In principle, for stratified physical situations, a knowledge of the sound speed profile and frequency spectrum of a transmitted signal allows the prediction of the received signal by normal-mode theory. In practice, the nonuniformity of the real environment means that this ideal cannot usually be acheived. In our case we were fortunate to find an experimental site for which the bottom is flat, horizontal, and uniform. In addition, the velocity profile was independent of depth at the time of the experiment. Therefore, the analysis was greatly simplified because analytic forms for the normal-mode functions could be used. Signal-to-noise ratios were greatly improved over those obtained for single pulse transmissions by the use of a continuous signal in which the pulses are delineated by pseudorandom phase changes. This procedure gives an average signal level which is comparable to that of a cw transmission and, in addition, enables us to average over many identical pulse transmissions.

In the following sections we describe our experiment and results. The standing wave patterns characteristic of normal modes are observed. An improved mode enhancement technique is described and its effectiveness in extracting the signal associated with a single normal mode is demonstrated. The technique is used to show that modes are strongly attenuated at frequencies near cutoff. Spectra of individual modes are obtained and the modifications due to attenuation and cutoff effects are observed. In all results there is good agreement with theoretical calculations.

I. NORMAL-MODE ACOUSTIC SIGNALS

The derivation of the acoustic pressure in a stratified water layer as an expansion in normal modes is well known,[4] and will not be repeated. The result can be written

$$p(r,z,t) = i\pi Q \sum_n u_n(z_0)u_n(z)H_0^{(1)}(k_n r)e^{-i\omega t}, \qquad (1)$$

where the acoustic pressure p is a function of range r, depth z, and time t. The acoustic source of strength Q is located at the point $r=0$, $z=z_0$ and emits harmonic waves of angular frequency ω. The normal modes $u_n(z)$ represent standing wave solutions to the depth-dependent part of the wave equation. The mode $u_n(z)$ has n antinodes between surface and bottom and represents

[a]Defence Scientific Establishment, HMNZ Dockyard, Devonport, Auckland, New Zealand.

[b]Cooley Electronics Laboratory, Department of Electrical and Computer Engineering, University of Michigan, Ann Arbor, Michigan 48109.

acoustic energy trapped within the water column. The so-called continuous modes have been omitted from Eq. (1) since their energy is rapidly absorbed in the bottom. Continuous modes are unimportant except at very short ranges.[5] The radial part of the wave equation has the Hankel function $H_0^{(1)}(k_n r)$ as solution. For large values of $k_n r$, the Hankel function is approximately an outgoing cylindrical wave with wave number k_n.[6] Each normal mode can be pictured as a vertical standing wave pattern which propagates radially away from the source.

Time-dependent signals may be treated by analysis in terms of frequency components. Each frequency component gives an expression like Eq. (1), and the results may be integrated over frequency to obtain the expected time-dependent signal. If the source emits a time-dependent signal $f(t)$ with spectrum $F(\omega)$ found by taking the Fourier transform, the received signal becomes

$$p(r,z,t) = i\pi Q e^{i\pi/4} \sum_n \int_{-\infty}^{\infty} u_n(z_0) u_n(z) \times (2/\pi k_n r)^{1/2} e^{ik_n r} F(\omega) e^{-i\omega t} d\omega . \quad (2)$$

The interpretation of Eq. (2) can be simplified somewhat by assuming that the frequency spectrum is narrow enough to ignore the frequency dependence of the normal-mode functions $u_n(z)$. With this approximation, Eq. (2) can be rewritten as

$$p(r,z,t) \approx \sum_n m_n(r,t) u_n(z) , \quad (3a)$$

where

$$m_n(r,t) = i\pi Q e^{i\pi/4} u_n(z_0) \int_{-\infty}^{\infty} (2/\pi k_n r)^{1/2} F(\omega) e^{i(k_n r - \omega t)} d\omega . \quad (3b)$$

The expected structure of normal-mode signals is clearly shown in Eqs. (3). Each term of the summation has two factors which separate the vertical and horizontal dependence of the pressure field. The depth dependence is contained in the normal-mode function $u_n(z)$. The radial dependence is contained in the factor $m_n(r,t)$, which represents a wave packet with spectrum $F(\omega)$. This wave packet propagates with group velocity $d\omega/dk_n$ which is different for each term. The amplitude of the wave packet in each mode depends on $u_n(z_0)$, the value of the mode at the depth of the source. This is expected physically since a mode will be strongly excited if the source is at an antinode.

If we now assume that the transmission is a short pulse, the pulses given by each mode coefficient $m_n(r,t)$ travel at different speeds and so become separated in time. Each arrival will have depth dependence characteristic of the associated normal mode; that is, it will have well-defined maxima and minima with the maxima alternating with phase as the depth changes. This expected variation with depth and time of the received signals was confirmed by the experiments of Eby *et al.*[7] in a laboratory tank and by Ferris and Ingenito[2,3] in the ocean.

II. THE EXPERIMENT

The site chosen for the experiment is about 18 km off shore from the University of Auckland Marine Laboratory at Leigh, 64 km north of Auckland. The main advantage of this site is that it has almost constant water depth over a large area 20 × 12 km. The bottom structure had been studied in a geological survey and consists of a layer of sand 100 m thick overlying a sub-bottom of greywacke rock.[8]

The experiment was designed to follow as closely as possible the conditions of the classic Pekeris model[1] of shallow water propagation. Although mathematically simple, the two isovelocity fluid model is a good approximation for low-order modes which do not penetrate to the sub-bottom and allows the normal modes to be obtained as analytic functions.

At the time of the experiment near-perfect isovelocity conditions prevailed. Parameter values for the experiment were the following:

water depth H	$= 50 \pm 1$ m,
tidal range	$= 3$ m,
sound speed in water C_1	$= 1508.7 \pm 0.3$ m s^{-1},
sound speed in bottom C_2	$= 1610 \pm 20$ m s^{-1},
bottom density ρ_2	$= 1500 \pm 300$ kg m^{-3}, and
range	$= 5.1 \pm 0.1$ km.

Acoustic signals were transmitted from a low-frequency source tunable in the range 50–150 Hz suspended at a depth of 6 m from HMNZS TUI (AGOR-5). The transmitted signals were essentially four-cycle sine wave pulses. This pulse length was selected as a compromise between the desire to obtain time resolution of normal modes in the received signals and the need for narrow bandwidth to simplify the theoretical analysis.

The signals were received by a vertical string of six hydrophones spaced at 7-m intervals between surface and bottom. The array was hardwired back to a small ship at anchor and the signals were recorded on magnetic tape together with a sampling synchronization signal telemetered from the transmitting site.

The frequency spectrum of a gated four-cycle sine wave of frequency f_0 is the familiar $|\sin x/x|$ function with its first nulls at $\frac{3}{4} f_0$ and $\frac{5}{4} f_0$. The electronic signals were bandpass filtered between these nulls before being passed to the source. This restricted the bandwidth as intended but also removed the sharp discontinuities at the ends of the pulse and their undesirable effects on the source.

In order to improve the signal-to-noise ratio of the recordings, a method of pulse compression was used. Previously, whenever pulsed transmissions have been used the pulses have been well separated in time so that the multiple arrivals usually obtained do not overlap with those of adjacent pulses. With this method the average power transmitted through the water is low and it is necessary to perform signal averaging over many

pulses. Accuracy is severely reduced if the propagation conditions vary in time as they normally do. The technique of pulse compression used here was to transmit four-cycle pulses continuously with each pulse distinguished from the previous not by a time gap but by a phase change. The phase changes form a pseudorandom repeating sequence and the average power of such a signal is comparable to that of a cw transmission. A knowledge of the sequence enables the recorded signals to be decoded and the response for a single transmitted pulse extracted. The decoding is performed in a digital computer after first digitizing the recorded signals. This decoding is equivalent to pulse averaging, and for a typical run at 100 Hz recording for 1 min provides averaging over 1500 four-cycle pulses. Pulse compression thus allows the use of power levels equivalent to continuous transmission while still allowing multiple-pulsed arrivals to be studied. The details will be discussed in a separate paper.

III. RESULTS AND ANALYSIS

A. Hydrophone waveforms

Data runs using the pulse compressed signals were recorded for center frequencies from 60 to 140 Hz in steps of 10 Hz. The records were digitized and computer processed to obtain the averaged results for a four-cycle source pulse. Figure 1 shows the processed records for 60, 100, and 140 Hz. These are representative of all runs. Mode cutoff frequencies for this situation calculated from the Pekeris model are 22, 66, 110, and 154 Hz for modes 1, 2, 3, and 4, respectively. Therefore, we expect to see one mode at 60 Hz, two modes at 100 Hz, and three modes at 140 Hz. It is clear from the records that the three sets of data do indeed show one, two, and three arrivals, respectively. The depth dependence of the three arrivals clearly identifies modes 1, 2, and 3 arriving in order. The first arrival has maximum amplitude at midwater depth and no nulls. The second arrival at 100 and 140 Hz has a minimum amplitude on the fourth hydrophone down, and the portions of the arrival above and below this depth have opposite phases. This depth dependence is characteristic of the second normal mode with two maxima in antiphase and a node at about midwater depth. Similarly, at 140 Hz the third arrival has three maxima alternating in phase and two nodes characteristic of the third mode.

Graphs similar to our result at 100 Hz were published by Ferris[2] showing two modes though several were expected. Our results show the systematic appearance of higher modes as the frequency is raised and demonstrate the suppression of noise obtained by the pulse compression technique. Further discussion of the hydrophone waveforms will be left until we have described the results of mode enhancement to pick out the arrivals associated with each mode.

B. Mode enhancement–theoretical

It is well known that the normal-mode functions $u_n(z)$ of Eq. (2) are orthogonal functions. Thus in principle the coefficient of a given normal mode in a linear combination of such modes can be obtained by simply multiplying by the desired mode and integrating over depth. Contributions from all other modes vanish in the usual way because of orthogonality. The acoustic pressure given by Eq. (3) is such a linear combination of normal modes, and we might attempt to extract the contribution of a single mode in the same manner.

There are two reasons why this may not work well. Firstly, the functions $u_n(z)$ are orthogonal for integration over z, i.e.,

$$\int_0^\infty u_n(z)u_m(z)dz = \delta_{mn}\,. \tag{4}$$

However, in a practical situation the acoustic pressure is sampled at discrete depths so that the integral in Eq. (4) is replaced by the summation

$$\sum_i u_n(z_i)u_m(z_i)\Delta z_i\,,$$

where the z_i are the depths of the hydrophones and Δz_i their spacing. With this replacement, Eq. (4) becomes only approximate, and typical results give numbers of order 1.0 if $m=n$ and of order 0.1 if $m\neq n$. Thus this

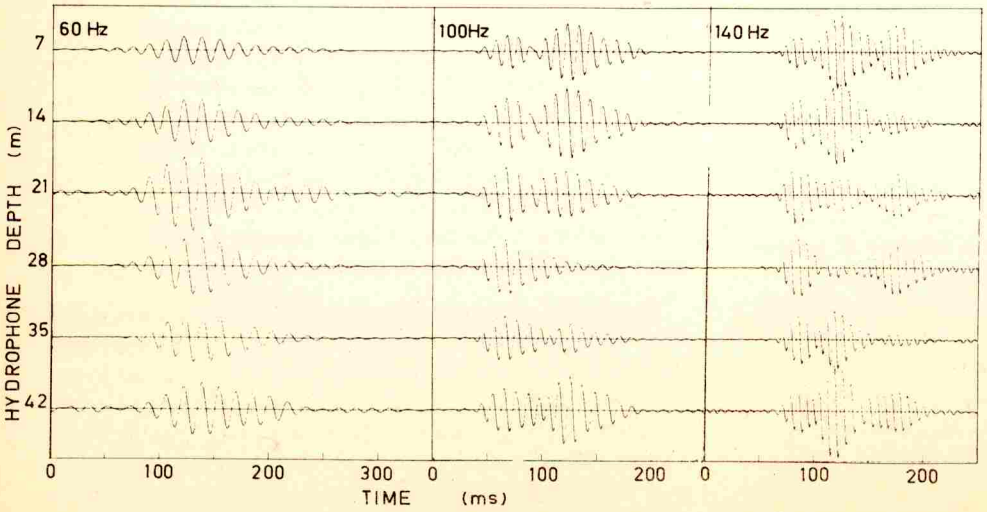

FIG. 1. Hydrophone waveforms received at 5.1 km. Source pulse four-cycle tone burst at frequencies shown. Acoustic pressure is plotted vertically in arbitrary units.

method of mode enhancement gives incomplete rejection of unwanted modes, and the enhanced results automatically contain admixtures of other modes.

The second reason why use of the orthogonal integration may not be successful concerns the approximation used to replace Eq. (2) by Eq. (3). It was necessary to neglect the frequency dependence of the normal-mode functions $u_n(z)$. This dependence is actually quite slight for the present model and is manifest as a steady change of the vertical spacing of nodes for each normal-mode function. For bandwidths which are not too great the frequency dependence may be neglected.

The usefulness of the orthogonality integral as a method of mode enhancement is therefore degraded by the necessity for discrete sampling. However, the integral was used by Ferris and Ingenito[2,3] to distinguish modes which were not resolved on analog records.

The difficulty associated with use of the orthogonality integral for mode enhancement can be avoided by recourse to matrix theory. Using the definitions

$$p_j = p(r, z_j, t),$$

$$u_{jn} = u_n(z_j),$$

where z_j is the depth of the jth hydrophone, Eq. (3a) may be rewritten

$$p_j = \sum_n u_{jn} m_n, \tag{5a}$$

or, in terms of the matrix U and column vectors $\mathbf{p}$ and $\mathbf{m}$, we have

$$\mathbf{p} = U\mathbf{m}. \tag{5b}$$

The vector $\mathbf{p}$ represents the signals received on the hydrophones and $\mathbf{m}$ represents the signals carried by individual modes. In the experimental situation $\mathbf{p}$ is measured and the matrix U may be calculated from the theoretical model. Therefore, Eq. (5) can be regarded as a system of linear equations to be solved for $\mathbf{m}$, the normal-mode signals.

The solution of Eq. (5) depends on the number of hydrophones and modes present.

If the number of hydrophones is equal to the number of modes, the matrix U is square and the solution of Eq. (5) is obtained by finding U^{-1}, the inverse of U, where $\mathbf{m} = U^{-1}\mathbf{p}$.

If there are more modes than hydrophones, there are effectively more unknowns than equations and so a unique solution does not exist.

The interesting case is where there are more hydrophones than modes. In this case the matrix U could be made square by discarding a suitable number of hydrophone records, but this would waste information. A better procedure is to obtain a "best fit" to the system as it stands. This is obtained by finding the matrix $(U'U)^{-1}U'$, where U' is the transpose of U. This new matrix is the Moore–Penrose pseudoinverse of the matrix U, and by using it to multiply Eq. (5b) we obtain the least-squares best fit solution for $\mathbf{m}$.[9] This gives

$$\mathbf{m} = (U'U)^{-1}U'\mathbf{p}. \tag{6}$$

Equation (6) allows extraction of the mode signals for an arbitrary number of hydrophones. The matrices are readily found from the theoretical model, and our results in later sections confirm the usefulness of Eq. (6).

Before returning to the experimental analysis we make two comments. Firstly, we note that the use of the orthogonality integral of Eq. (4) to extract the normal-mode signals is equivalent to multiplying Eq. (5) by U', i.e.,

$$U'U\mathbf{m} = U'\mathbf{p}. \tag{7}$$

As we have already mentioned the matrix $U'U$ has diagonal elements which are near 1.0 and off-diagonal elements which are of order 0.1, i.e., near zero. Thus $U'U$ is close to the unit matrix, and hence from Eq. (7)

$$\mathbf{m} \approx U'\mathbf{p},$$

giving an approximate solution to the problem. It is now easily seen by comparing Eqs. (6) and (7) that use of the pseudoinverse avoids this approximation by multiplying Eq. (7) by $(U'U)^{-1}$ to obtain Eq. (6).

The second comment is that the use of a hydrophone array to enhance a particular normal mode is similar to beamforming. Normal modes can be considered as the interference pattern due to upgoing and downgoing rays at the same angle. The mode-enhancement matrices are weighting functions for the hydrophones which "steer" the array in the direction of these rays. The improvement using the pseudoinverse matrix rather than the orthogonality integral is due to an improved beam pattern which suppresses unwanted modes by arranging for nulls at the appropriate angles. Further work on the correspondence with beamforming is in progress.

C. Mode enhancement—experimental

The technique of mode enhancement is readily applied to the experimental data. The vector $\mathbf{p}$ of Eq. (6) represents the time dependent signals received on the six hydrophones. These waveforms are available as digital computer files as a result of the signal processing. The elements of the matrix U defined in Eqs. (5) are the theoretical mode amplitudes at the depths of the hydrophones. These are found for the present situation by finding the normal modes of the Pekeris model with the appropriate parameters. The matrix $(U'U)^{-1}U'$ of Eq. (6) is then constructed for each value of center frequency used in the experiment and the matrix is stored in a computer file. A computer program based on Eq. (6) yields time-dependent signals $\mathbf{m}$ which are weighted combinations of the hydrophone signals $\mathbf{p}$ and which are least-squares best fits to the normal-mode signals.

The initial attempts at mode enhancement were somewhat disappointing in that each normal mode apparently showed the same multiple arrivals present in the hydrophone waveforms. The source of this difficulty was attributed to a slight time shift from hydrophone to hydrophone. This was just observable on the computer plots as a very slight shift of the waveform carrier phase as

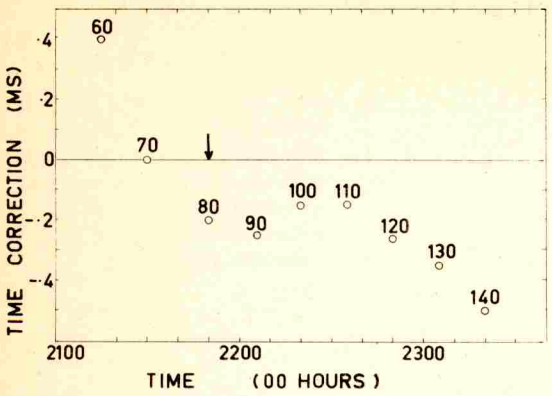

FIG. 2. Time correction per hydrophone required for best mode enhancement plotted against time of day. High water is indicated by the arrow. Points are labeled by center frequencies of transmission.

the depth changes. It is assumed that this time delay occurs because our hydrophone string is not quite vertical but is leaning over in any tidal flow.

To remove this effect it was assumed that the time shift from hydrophone to hydrophone was linear, and arbitrary adjustments were made until good separation of the modes was obtained. The improvement was quite definite, and the time shift required was easily determined to within 0.01 ms. The time corrections are shown in Fig. 2 plotted as a function of time of day during the experiment. The maximum time correction corresponds to a deviation from vertical of about 6° for the hydrophone string. There is a steady change of angle throughout the experiment, which agrees roughly with the time of local high water as indicated by the arrow. The results indicate that the hydrophone string swings away from vertical and then recovers slightly between 2220 and 2240 h before swinging away again. This possibly indicates the passage of a perturbation of the tidal flow. Unfortunately, there are no detailed measurements of tidal flow in the area, and the flow pattern could not be checked.

Typical results from the mode enhancement are shown in Fig. 3. The signals present in each normal mode are shown as a function of time for three different center frequencies. As mentioned in connection with Fig. 1, we expect one, two, and three modes, respectively, at the frequencies shown, and this is indeed observed.

It will be noticed that separation of the modes is not perfect. At 60 Hz the signal obtained for mode 2 is due to incomplete rejection of mode 1. Similarly, at 140 Hz there is incomplete rejection of unwanted modes, each mode signal showing small amounts of "cross talk" from other modes. This imperfect mode separation is probably due to our unavoidable approximation that the mode functions are independent of frequency. The only situation we found where mode enhancement failed to give a clear identification of the pulse associated with a given mode was at 70 Hz, where the waveform for mode 2 always showed intereference from mode 1.

In spite of the slight imperfections in the mode enhancement, it is clear that in general mode separation is very good, and the pulse shapes and arrival times associated with each mode can be easily studied. This is in contrast to the hydrophone waveforms of Fig. 1, where mode interference considerably distorts the pulse shapes.

IV. COMPARISON WITH THEORY

A. Group velocities

Resolution of the received signals into pulses associated with each normal mode enables us to measure relative arrival times quite accurately. This can be done more accurately from the separated mode waveforms than from the multiple arrivals present on the hydrophone signals of Fig. 1.

The arrival time of a pulse is taken from the plotted results as the time when the envelope of the pulse has maximum amplitude. This can be readily found by selecting the cycle of greatest amplitude. If it happens that adjacent positive and negative half cycles have the same amplitude the time is taken from the zero crossover in between. In this way the pulse arrival time can be found with an estimated error of a quarter of the period of the carrier.

For our purposes it is unnecessary to measure absolute arrival times, since the relative arrival times are much more sensitive to the details of the physical model. The points plotted in Fig. 4 show the arrival times of modes 2 and 3 relative to mode 1 as a function of the center frequency of the transmission. Theoretical values for the relative arrival times are given by the dashed curve of Fig. 4. They are calculated from the Pekeris

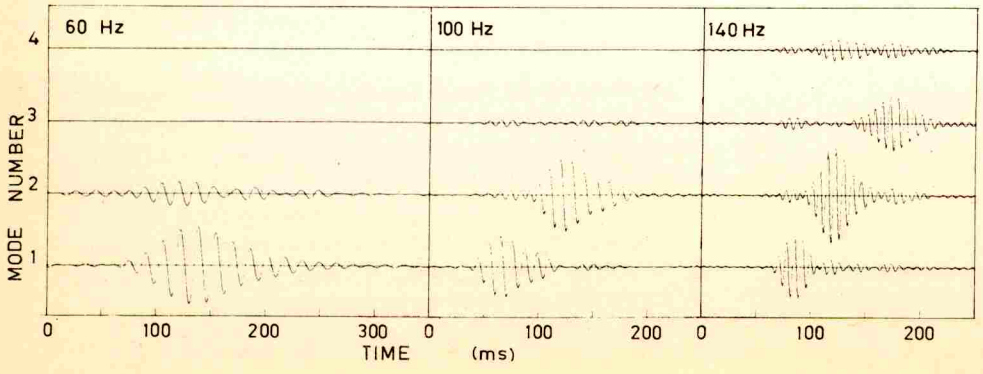

FIG. 3. Normal-mode waveforms obtained by mode enhancement of the records of Fig. 1.

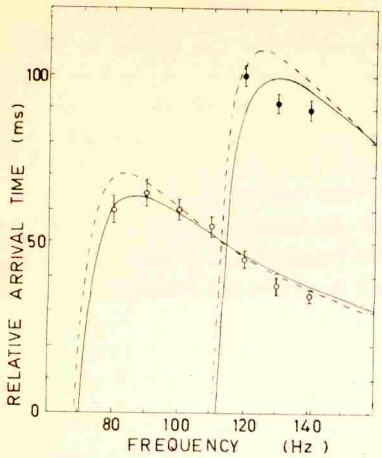

FIG. 4. Relative arrival times of normal modes as a function of frequency. The circles show the measured arrival time of mode 2 relative to mode 1, and the dots show mode 3 relative to mode 1. The dashed curve shows the theoretical time differences derived using the original values for sound speed and density of the bottom. The solid curves show an improved fit obtained by adjusting the parameters.

model using the bottom parameters ρ_2 and c_2 obtained from the seismic survey. Adjustment of these parameters within their quoted errors yields the solid curve of Fig. 4, which is a much better fit to the data. The adjusted values are

$$\rho_2 = 1250 \text{ kg m}^{-3}, \quad c_2 = 1605 \text{ m s}^{-1},$$

and these were used for the subsequent analysis.

Adjustment of the parameters of the model necessitated alterations of the matrices and reprocessing of the hydrophone data to obtain the normal mode signals. However, this did not alter the relative arrival times and further adjustment was unnecessary.

The fitting of these curves should not be regarded as a definitive determination of ρ_2 and c_2 for two reasons. Firstly, a Pekeris model has been assumed (i.e., that the bottom is semi-infinite and uniform). The general agreement of theoretical and experimental values indicates the validity of the model but does not rule out the possibility that more complicated layering is present.

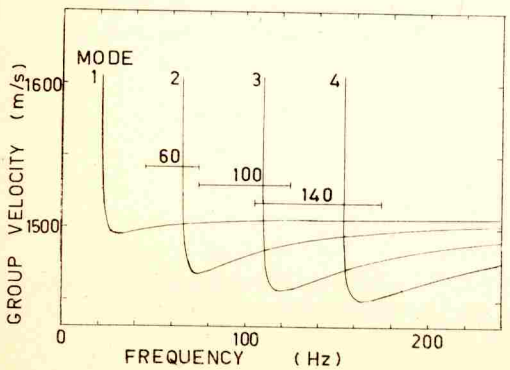

FIG. 5. Theoretical curves for group velocity as a function of frequency for the first four modes. The bandwidths assumed for four-cycle pulses at 60, 100, and 140 Hz are indicated.

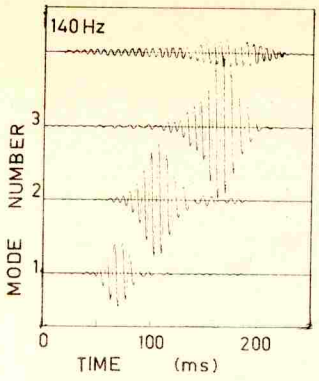

FIG. 6. Theoretical normal-mode waveforms at 140 Hz. The figure is to be compared with the 140-Hz experimental waveforms of Fig. 3 and is normalized to give the same amplitude for mode 1.

Secondly, the penetration of normal modes into the bottom is usually very slight so that the parameters obtained are representative of only the uppermost few meters of the bottom.

B. Mode waveforms

Dispersion is due to variation of group velocity with frequency and leads to distortion of pulse shapes as the pulses propagate. Two dispersion effects are observed in Fig. 3 and both can be understood with reference to Fig. 5, which shows the theoretical mode group velocities as a function of frequency. Figure 5 also shows the bandwidths appropriate to the data of Fig. 3.

Firstly, consider the group velocities for the 140-Hz data. Figure 5 shows that within the bandwidth at 140 Hz the group velocity of mode 1 is almost constant. Thus all frequency components travel at the same speed and there should be very little pulse spreading. This is verified in Fig. 3, where the pulse in mode 1 at 140 Hz is very short, being essentially the same width as the source pulse. The group velocities of modes 2 and 3 at 140 Hz show more variation than mode 1 within the bandwidth. Indeed, cutoff for mode 3 occurs at 110 Hz, and there is very rapid change of group velocity. Thus modes 2 and 3 have successively wider ranges of group velocities than mode 1, and this should give successively greater pulse spreading. This is again verified by Fig. 3, and we conclude that for our experimental situation pulse spreading increases as mode number increases.

Secondly, Fig. 3 shows that near 60 Hz the group velocity for mode 1 is changing more rapidly than it is near 140 Hz and the range of group velocities is correspondingly larger. Therefore, dispersion should lead to greater spreading at 60 than at 140 Hz. This is also verified by Fig. 3, in which the pulse in mode 1 is about 9, 7, and 5 cycles long for 60, 100, and 140 Hz, respectively. We conclude that pulse spreading for a given mode increases as the frequency decreases.

The theoretical result for the mode waveforms is found by calculating $m_n(r,t)$ from Eq. (3) using our Pekeris model of the sound channel. Results at 140 Hz are shown in Fig. 6, which may be compared with the experimental results of Fig. 3. For the first three modes agreement between relative arrival times and pulse lengths is very good. Indeed, this is the case for all data runs, so there is no advantage in showing all our results.

There are two respects in which the experimental and theoretical waveforms differ. Firstly, the relative amplitudes of the first three modes do not agree. This is due entirely to the fact that our theoretical model makes no allowance for attenuation. The theoretical curves have been arbitrarily normalized so that theoretical and experimental amplitudes of mode 1 are the same. Thus, the reduced amplitudes for the experimental results for modes 2 and 3 indicate attenuation which increases with mode number. Greater attenuation of higher modes is expected physically, since the higher modes penetrate further into the bottom layer where the absorption of acoustic energy takes place.

The second respect in which theoretical and experimental waveforms disagree concerns mode 4 and is the subject of Sec. IV C.

C. Normal modes near cutoff

Each normal mode has a low-frequency cutoff below which it does not form a discrete standing wave and its energy ceases to be trapped in the water column. The presence of a cutoff frequency is indicated by the abrupt termination at the low-frequency end of the group velocity curves of Fig. 5.

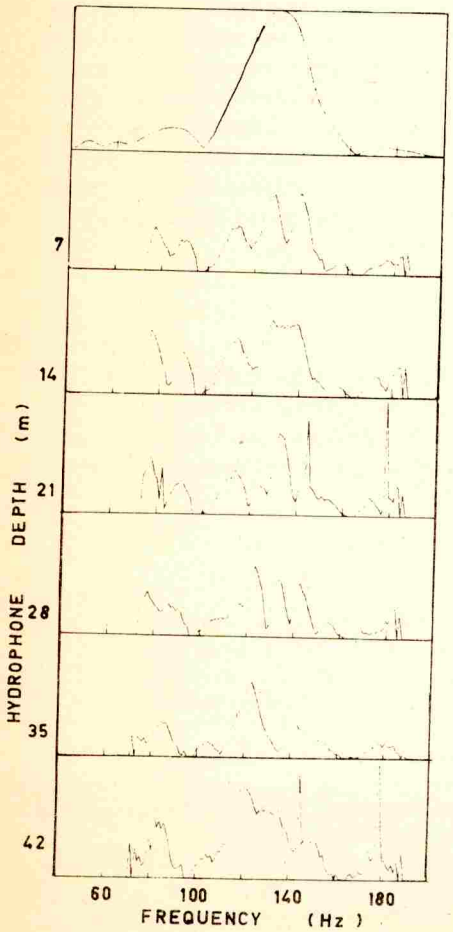

FIG. 7. Pulse frequency spectra obtained on the hydrophones at 130 Hz. Vertical scale is arbitrary and the hydrophones were at the depths indicated. The top graph shows the spectrum of the source pulse for comparison.

It is tempting to assume that a normal mode will propagate if the signal frequency exceeds the cutoff frequency for that mode. However, the situation is not that simple. For pulsed transmissions a finite bandwidth is implied and has been indicated on Fig. 5 for representative cases. Thus, the bandwidth as shown for a four-cycle pulse with a center frequency of 140 Hz overlaps with the group velocity curve for mode 4 and indicates that mode 4 should be observed in the 140-Hz data even though its cutoff frequency is 154 Hz. The theoretically expected pulse shape is shown in Fig. 6. The pulse should suffer considerable time spreading because of the wide range of group velocities present.

The experimental results for mode 4 at 140 Hz as shown in Fig. 3 do not agree with the theoretical results of Fig. 6. The waveform obtained for mode 4 shows pulses which are strongly correlated with those for lower modes and is probably due to imperfect mode enhancement. The presence of any genuine mode 4 is obscured by the cross talk due to other modes. Similarly, the bandwidths at 60 and 100 Hz indicate that theoretically modes 2 and 3 are expected in those runs. However, these are not observed in Fig. 3, where there is no mode 3 at 100 Hz, and the waveform for mode 2 at 60 Hz is probably again due to cross talk.

It is almost certainly because of the attenuation seen in the previous section that we do not observe modes whose cutoff frequencies are above the center frequencies of the pulses. The higher modes suffer greater attenuation because of their greater penetration into the bottom. Thus a mode which is just cut off will necessarily have severe attenuation of all its components and at sufficient range will not be seen.

D. Frequency spectra

The frequency spectra of broadband signals received in underwater acoustics are usually quite complicated. Figure 7 shows the spectra received on our six hydrophones for a source pulse of center frequency 130 Hz.

The spectrum of the source pulse is also shown in the figure. The source pulse spectrum is quite simple and has the characteristic $|\sin x/x|$ shape of a gated sine wave. With four-cycle pulses the first nulls for a center frequency of 130 Hz occur at 97.5 and 162.5 Hz as in the figure. The signals were bandpass filtered between these points before sending to the source, but there is some signal outside because of rolloff in the filters and because the source has a resonance at 67 Hz which gives the enhanced lower side lobe.

It is difficult to draw detailed conclusions from such complicated spectra as those observed on the hydrophones. The spectra all have the gross shape of the source pulse. There is, however, severe departure from this gross shape giving sharp nulls in several cases. From our earlier results it is clear that these nulls are caused by the interference of pulses from different modes. Each frequency component in each mode has its own phase and amplitude. Thus components from different modes may cancel out if they have

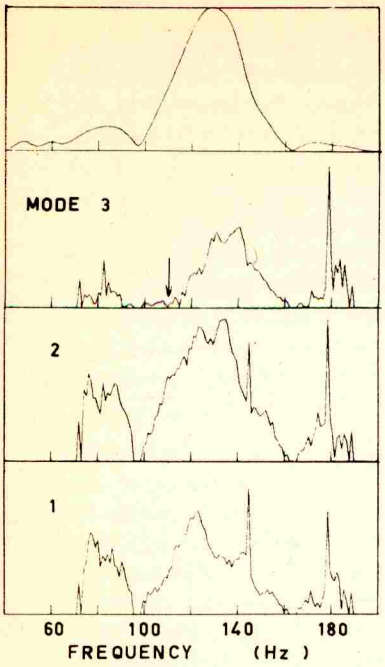

FIG. 8. Pulse frequency spectra for individual normal modes obtained by mode enhancement of the records of Fig. 7. The top graph shows the spectrum of the source pulse. The arrow indicates mode 3 cutoff at 110 Hz.

opposite phase, giving minima in the frequency spectrum.

The mode-enhancement technique described earlier enables us to pick out from the multiple arrivals the pulse associated with a single mode and to examine its spectrum. Typical results are shown in Fig. 8, which is also for a center frequency of 130 Hz. The source pulse is again shown for comparison. Mode enhancement and Fourier transformation are both linear processes, so Fig. 8 can be regarded as the result of applying mode enhancement to the spectra of Fig. 7. The mode spectra are much simpler than the hydrophone spectra and are easier to interpret.

Consider firstly the spectra of modes 1 and 2. Their cutoff frequencies are too low to affect the spectrum of a 130-Hz, four-cycle pulse. The resulting spectra are thus expected to be the same as that of the source pulse. Agreement is quite good; the irregularities are due to noise and to imperfections in the mode enhancement. Cutoff frequency for mode 3 is 110 Hz and is indicated by the arrow in the diagram. The theoretical spectrum for mode 3 obtained from a Pekeris model with no attenuation would be expected to be as for the source pulse above 110 Hz but dropping abruptly to zero below this cutoff frequency. The results in Fig. 8 show fairly definitely that mode 3 has negligible components below 110 Hz especially when compared with the source pulse and modes 1 and 2. However, the cutoff of components below 110 Hz does not occur suddenly at 110 Hz as the model would suggest. It can be seen from Fig. 8 that attenuation begins above cutoff frequency and increases rapidly as cutoff is approached, as was concluded earlier from the measured mode amplitudes.

V. CONCLUSIONS

The experiment and analysis described here has confirmed in detail the theoretically expected frequency dependence of normal modes.

The assumption that the sand forming the bottom layer of our experimental site can be regarded as a semi-infinite fluid is well justified.

The only deficiency of our mathematical model is its obvious failure to include the effects of attenuation. Our results show that attenuation increases rapidly near cutoff frequencies. However, it is quite clear that many of the features of normal-mode transmission can be accounted for without allowing for attenuation in the theoretical model.

The method of mode enhancement suggested here is shown to allow the extraction of the signal associated with a single mode. This greatly facilitated the determination of group velocities and the study of mode waveforms and spectra. The method was applied here to particularly simple data which were already partly separated into mode pulses and for which the results of mode enhancement could be easily anticipated. The great advantage of the method is, however, that it is expected to work just as well on data in which modal arrivals are not well resolved, either because the range is too short or because the transmitted signal is too long or too complicated. Since the signal in each mode is substantially a facsimile of the transmitted signal, the method offers the possibility of extracting the transmitted signal from the usual succession of overlapping multiple arrivals. A particularly interesting application will be the study of mode coupling due to range-dependent features such as a sloping bottom.

ACKNOWLEDGMENTS

The authors gratefully acknowledge the assistance of the Defence Scientific Establishment for the provision of shipping time, the cooperation of the personnel of HMNZS TUI and the encouragement and support of Professor A. C. Kibblewhite.

[1]C. L. Pekeris, Geol. Soc. Am., Mem. 27, (1948).
[2]R. H. Ferris, J. Acoust. Soc. Am. **52**, 981–988 (1972).
[3]F. Ingenito, J. Acoust. Soc. Am. **53**, 858–863 (1973).
[4]I. Tolstoy and C. S. Clay, *Ocean Acoustics* (McGraw–Hill, New York, 1966).
[5]C. T. Tindle, A. P. Stamp, and K. M. Guthrie, J. Sound Vib. **49**, 231–240 (1976).
[6]*Handbook of Mathematical Functions*, edited by M. Abramowitz and I. A. Stegun (Dover, New York, 1965).
[7]R. K. Eby, A. O. Williams, Jr., R. P. Ryan, and P. Tamarkin, J. Acoust. Soc. Am. **32**, 89–99 (1960).
[8]S. R. Ferguson, "The velocity structure of the sea bed and basement rocks between Leigh and Mokohinau," M.Sc. thesis (Univ. Auckland, 1974).
[9]G. W. Stewart, *Introduction to Matrix Computations* (Academic, New York/London, 1973), p. 221.

DISTRIBUTION LIST - 1

	No. of Copies
Office of Naval Research Department of the Navy Arlington, Virginia 22217 Attn: Code 222	2
102-OS	1
480	1
Director Naval Research Laboratory Technical Information Division Washington, D.C. 20375	6
Director Office of Naval Research Branch Office 1030 East Green Street Pasadena, California 91106	1
Office of Naval Research San Francisco Area Office 760 Market Street - Room 447 San Francisco, California 94102	1
Director Office of Naval Research Branch Office 495 Summer Street Boston, Massachusetts 02210	1
Office of Naval Research New York Area Office 207 West 24th Street New York, New York 10011	1
Director Office of Naval Research Branch Office 536 South Clark Street Chicago, Illinois 60605	1
Commander Naval Surface Weapons Center Acoustics Division White Oak Silver Springs, Maryland 20910 Attn: Dr. Zaka Slawsky	1
Commanding Officer Office of Naval Research Branch Office Box 39 FPO New York 09510	1

Officer in Charge
Naval Ship Research & Dev. Center
Annapolis Laboratory
Annapolis, Maryland 21402 — 1

Commander
Naval Sea Systems Command
Department of the Navy
Washington, D.C. 20362
Attn: SEA 037
Carey Smith, 06HI — 1
David F. Bolka, 06H2 — 1

Commanding Officer
Fleet Numerical Weather Central
Monterey, California 93940 — 1

Defense Documentation Center
Cameron Station
Alexandria, Virginia 22314 — 12

Director of Navy Laboratories
Chief of Naval Material
2211 Jefferson Davis Highway
Crystal Plaza #5
Arlington, Virginia 20360
Attn: Dr. James Probus NAVMAT 03L — 1

Commander
Naval Electronic Systems Command
2511 Jefferson Davis Highway
Arlington, Virginia 20360
Attn: CDR A.R. Miller NAVELEX 320 — 1

Commander Naval Ship Research & Development Center
Department of the Navy
Bethesda, Maryland 20084
Attn: Mr. Craig Olson — 1
Unclassified Library — 1

Chief of Naval Operations
Room 4D518, Pentagon
Washington, D.C. 20350
Attn: CAPT A.H. Gilmore — 1

Commander
Naval Ocean Systems Center
Department of the Navy
San Diego, California 92132
Attn: Dr. Dan Andrews — 1
Mr. Henry Aurand — 1
Dr. Dean Hanna — 1

Superintendent
Naval Research Laboratory
Underwater Sound Reference Division
P.O. Box 8337
Orlando, Florida 32806 — 1

Commanding Officer
Naval Underwater Systems Center
New London Laboratory
New London, Connecticut 06320
Attn: Dr. A. Nuttall — 1
Mr. A. Ellinthrope — 1
Dr. D. M. Viccione — 1

Commander
Naval Air Development Center
Department of the Navy
Warminster, Pennsylvania 18974
Attn: Unclassified Library — 1

Superintendent
Naval Postgraduate School
Monterey, California 93940
Attn: Unclassified Library — 1

Commanding Officer
Naval Coastal Systems Laboratory
Panama City, Florida 32401
Attn: Unclassified Library — 1

Commanding Officer
Naval Underwater Systems Center
Newport Laboratory
Newport, Rhode Island 02840
Attn: Unclassified Library — 1

Superintendent
U.S. Naval Academy
Annapolis, Maryland 21402
Attn: Library — 1

Commanding Officer
Naval Intelligence Support Center
4310 Suitland Road
Suitland, Maryland 20390
Attn: Dr. Johann Martinek — 1
Mr. E. Bissett — 1

Office of the Assistant Secretary of the Navy
for Research, Engineering & Systems
Room 4E732, Pentagon
Washington, D.C. 20350
Attn: Mr. Gerald Cann — 1

Commander Naval Sea Systems Command Washington, D.C. 20362 Attn: Unclassified Library, SEA 03E	1
Dr. Melvin J. Jacobson Rensselaer Polytechnic Institute Troy, New York 12181	1
Dr. Alan Winder MSB Systems, Inc. 25 Sylvan Road South West Point, Connecticut 06880	1
Dr. Charles Stutt General Electric Company P.O. Box 1088 Schenectady, New York 12301	1
Dr. T.G. Birdsall Cooley Electronics Laboratory University of Michigan Ann Arbor, Michigan 48109	1
Dr. Harry DeFerrari University of Miami Rosenstiel School of Marine & Atmospheric Sciences 4600 Rickenbacker Causeway Miami, Florida 33149	1
Mr. Robert Cunningham Bendix Electronics Center 15825 Roxford Street Sylmar, California 91342	1
Dr. Stephen Wolff John Hopkins University Baltimore, Maryland 21218	1
Dr. M. A. Basin S.D.P., Inc. 15250 Ventura Boulevard Suite 518 Sherman Oaks, California 91403	1
Dr. Walter Duing University of Miami Rosenstiel School of Marine & Atmospheric Sciences 4600 Rickenbacker Causeway Miami, Florida 33149	1

Dr. David Middleton
127 East 91st Street
New York, New York 10028 — 1

Dr. Donald W. Tufts
University of Rhode Island
Kingston, Rhode Island 02881 — 1

Dr. Loren Nolte
Duke University
Department of Electrical Engineering
Durham, North Carolina 27706 — 1

Mr. S. W. Autrey
Hughes Aircraft Company
P.O. Box 3310
Fullerton, California 92634 — 1

Dr. Thomas W. Ellis
Texas Instruments, Inc.
13500 North Central Expressway
Dallas, Texas 75231 — 1

Dr. Terry Ewart
Applied Physics Laboratory
University of Washington
1013 Northeast Fortieth Street
Seattle, Washington 98195 — 1

Institute for Acoustical Research
Miami Division of the Palisades
Geophysical Institute
615 S. W. 2nd Avenue
Miami, Florida 33130
Attn: Mr. M. Kronengold
Dr. J. Clark
Dr. W. Jobst
Dr. S. Adams — 4

Mr. Carl Hartdegen
Palisades Geophysical Institute
Sofar Station
FPO New York 09560 — 1

Mr. Charles Loda
Institute for Defense Analyses
400 Army-Navy Drive
Arlington, Virginia 22202 — 1

Special Assistant for ASW
Office of the Assistant Secretary of the Navy
for Research, Engineering & Systems
Washington, D.C. 20350
Attn: Dr. D. Hyde — 1

Mr. Beaumont Buck
Polar Research Laboratory
123 Santa Barbara Avenue
Santa Barbara, California 93101 — 1

Dr. M. Weinstein
Underwater Systems, Inc.
8121 Georgia Avenue
Silver Spring, Maryland 20910 — 1

Mr. Thomas G. Kincaid
General Electric Company
P.O. Box 1088
Schenectady, New York 12301 — 1

Applied Research Laboratories
University of Texas at Austin
P.O. Box 8029
10000 FM Road 1325
Austin, Texas 78712 — 2
Attn: Dr. Lloyd Hampton
Dr. Charles Wood

Woods Hole Oceanographic Institution
Woods Hole, Massachusetts 02543 — 1
Attn: Dr. Paul McElroy
Dr. R. Porter
Dr. R. Spindel

Mr. John Bouyoucos
Hydroacoustics, Inc.
321 Northland Avenue
P.O. Box 3813
Rochester, New York 14610 — 1

Ronald J. Carpinella (Major)
Wright-Patterson AFB
Dayton, Ohio 45433 — 1

Atlantic Oceanographic &
Meteorological Laboratories
15 Rickenbacker Causeway
Miami, Florida 33149 — 1
Attn: Dr. John Proni

Dr. C. N. K. Mooers
University of Delaware
Newark, Delaware 19711 — 1

Westinghouse Electric Corporation
Advanced Development Program
Marketing Department - MS 227
P.O. Box 746
Baltimore, Maryland 21203
Attn: F. J. Frissyn — 1

Oak Ridge National Laboratory
Union Carbide Corporation
Nuclear Division
P.O. Box X
Oak Ridge, Tennessee 37830 — 1

Professor Neil Bershad
University of California, Irvine
School of Engineering
Irvine, California 92664 — 1

Stuart Schwartz
Princeton University
Department of Electrical Engineering
Brackett Hall, Engineering Quad.
Princeton, New Jersey 08540 — 1

Ray Veenkant
Texas Instruments Inc.
North Central Expressway
MS 208
Dallas, Texas 75222 — 1

Dr. C. V. Kimball
University of Miami
Rosenstiel School of Marine &
Atmospheric Sciences
10 Rickenbacker Causeway
Miami, Florida 33149 — 1

Cooley Electronics Laboratory
University of Michigan
Ann Arbor, Michigan 48109 — 25